DEPOSITION OF Co NANOPARTICLES ON MESOPOROUS-SILICA SUPPORTS USING SUPERCRITICAL CO_2

A. Sastre[1], S. Aspromonte[2], A. Boix[2], M. J. Cocero[1], E. Alonso[1]
[1]High Pressure Processes Group. - Chemical Engineering and Environmental Technology Dept., Universidad de Valladolid, (Spain)
[2] Instituto de Investigaciones en Catálisis y Petroquímica – INCAPE (FIQ-UNL-CONICET), Santa Fe, (Argentina)
ealonso@iq.uva.es *Phone: +34 983 42 31 75* *Fax:+34 983 42 30 13*

INTRODUCTION

Mesoporous materials with uniform and tailorable pore dimensions and high surface areas, are currently being employed in a number of applications that include catalysis [1,2] and their used as templates for controlling the aspect ratio of quantum-confined nanoparticles and nanowires [3], among others. MCM41 is a mesoporous-silica material that contains unidirectional channels arranged in a regular hexagonal pattern in the range 15 -100 Å. In recent times, in the literature, it can be found attempts to insert transition metals [4], such as, Cu, Ca, Mg, Ti, Cr, Mn or Fe into the MCM41 framework, and this incorporation has been generally performed by wet impregnation or co-precipitation [5]. Supercritical fluid reactive deposition (SFRD) is an alternative technique in which an organometallic precursor is dissolved in supercritical carbon dioxide ($scCO_2$), and its subsequent decomposition allows the precipitation and deposition of metal or metal oxides over the mesoporous support. It takes advantage of the excellent physical properties of $scCO_2$, which are easily adjustable with small variations of pressure and/or temperature. The low viscosity, high diffusivity and zero surface tension of $scCO_2$ achieve better penetrating and wetting of pores than conventional liquid solvents. Furthermore, simple removal from the substrate by depressurization avoids problems of solvent residues or pore collapse. It is well known that the nature, dispersion and size of the metal nanoparticles are key factors in determining the activity and selectivity of the supported catalysts, and the use of $scCO_2$ as reaction medium improves dispersion on the support.

This work presents the deposition of Co nanoparticles into MCM41 and Al-MCM41 mesoporous matrix by SFRD. Several publications on cobalt oxide particles supported on mesoporous materials have reported good catalytic performance in the total oxidation of toluene [6, 7] and for the Fischer Tropsch reaction [8, 9].

This work presents the deposition of Co nanoparticles into MCM41 and Al-MCM41 by the decomposition of cobaltocene ($CoCp_2$) using supercritical carbon dioxide, and its subsequent characterization by means of different techniques, such as SEM/EDX, TEM, SAXS or Laser Raman Spectroscopy (LRS). Experimental results show the effect of precursor concentration on the obtained composite materials, and extended results can be found in [10].

EXPERIMENTAL SECTION

Synthesis of MCM-41 and Al-MCM-41

Mesoporous supports were synthesized in its spherical shape as reported by Szegedi et al [11]. 1 g of n-hexadecyltrimetilammoniumbromide (C_{16}TMABr) was dissolved in 19.2 g of de-ionized water and mixed with 24 g of absolute ethanol. 5.9 g of aqueous ammonia solution (29 wt%) were added and stirred for 15 min. Under stirring, 1.88 g of tetraethylorthosilicate (TEOS) were added drop-wise in a couple of minutes. The resulting powder having the molar composition of 1TEOS:0.3C_{16}TMABr:11NH_3:144H_2O:58EtOH was stirred for 2 h and aged for additional 16 h at 25 ºC. The white precipitates were filtered and washed several times until neutral pH was reached. Then the samples were dried for 12 hours at 60 ºC. The template removal was carried out by heating the samples in air up to 600 ºC at 1 ºC·min^{-1} heating rate.

Deposition of Co nanoparticles

Co/MCM41 and Co/Al-MCM-41 samples were synthesized by Supercritical Fluid Reactive Deposition (SFRD). Metal and cobalt oxide nanoparticles were synthesized and dispersed inside the mesoporous silica powder by thermal decomposition of the appropriating organometallic precursor in $scCO_2$. Cobalt (II) bis-(η^5-ciclopentadienil), also known as cobaltocene $CoCp_2$, was used as precursor because it is known to be highly soluble in $scCO_2$ [12], and has been utilized in the Co deposition of high purity thin films directly on silicon oxide [13]. $CoCp_2$ was obtained from Sigma Aldrich and used as received. CO_2 (99.99%) was supplied by Carburos Metálicos. At the beginning of each experiment 100 mg of mesoporous support were placed in a glass tube of 15 mm diameter, and the desired amount of arganometallic precursor ($CoCp_2$) into a second glass tube of smaller diameter (6 mm). Both glass tubes were placed in a 100 mL high-pressure reactor separated by wire mesh to allow the entrance and circulation of the $scCO_2$ and avoiding their direct contact, as it is shown in Fig. 1.

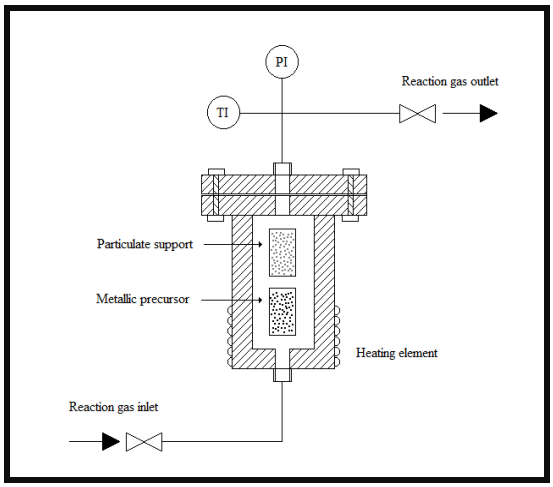

Figure 1. Experimental dispositive

The reactor is equipped with two wall electrical resistances and contains a K-Thermocouple connected to a controller for measuring and controlling the reactor temperature. Both resistors

are located at the bottom of the reactor to promote convective flow of $scCO_2$. Deposition experiments were carried out in batch operation divided in two consecutive stages. During the first step, the dissolution of the precursor $CoCp_2$ in $scCO_2$ and the impregnation of the support take place, and operational conditions are fixed at 70 °C and 11.0 MPa during 3 h. The second step is the decomposition and the deposition at 200 °C and 16.0 MPa. Afterwards, the $scCO_2$ was released from the reactor over a period of approximately 1 hour which implies a slowly depressurization to atmospheric pressure.

The amount of cobalt loading was represented with "X" in the Co(X)/MCM-41 and Co(X)/Al-MCM-41.

Characterization techniques

The real amount of metal loading into the supports was quantified by means of ICP-OES. Scanning Electron Microscopy (SEM) combined with detection by Energy Dispersive X-ray Spectroscopy (EDX) was performed to analyze the morphology of the support and to determine the chemical composition of the deposited particles. An environmental scanning electron microscope (ESEM) FEI Quanta model 200FEG operating at 30 kV was used. A JEOL field emission microscope model JEM-FS2200 HRP operating at 200 kV was also used to determine the organization, morphology and the pore dimensions, as well as to observe the presence of metallic particles dispersed within and/or out of the pores. In addition, this technique allows measuring the nanoparticles interplanar distance and analyzing the particle distribution by means of X-ray mapping. The BET surface area and pore size distribution were determined using a Micromeritics Accusorb 2100E instrument by the isotherms of adsorption and desorption of N_2. the materials were in contact with adequate amounts of N_2 to cover the whole range of relative pressures to near saturation (P/P_0=0.995). The X-ray diffraction patterns at low angle allow assessing the degree of structural arrangement of the prepared samples. Small Angle X-ray Scattering (SAXS) measurements were made at 2θ between 0º and 8º. Samples were also characterized by Laser Raman Spectroscopy (LSR) and **X**-ray Photoelectron Spectroscopy (XPS) to identify metallic species.

RESULTS AND DISCUSSION

Effect of precursor concentration and support material

Previous to the deposition experiments, two samples of mesoporous suppors were located inside the high-pressure reactor at 200 ºC and 160 bar during 6 h in order to test the effect of pressure and temperature on the bare supports. No significant changes were observed in terms of ABET and pore diameter, and TEM images of ''fresh'' and ''CO_2-treated'' supports showed similar hexagonal patterns.

Deposition experiments started at 70 ºC and 11.0 MPa for a period of 3 h to guarantee dissolution of the $CoCp_2$ precursor in $scCO_2$ and impregnation of the support. High solubility, good mass transfer properties and good adsorption were desirable during this period. Adsorption was favoured at low pressures, and $CoCp_2$ solubility in CO_2 increased with density, as was described by Aschenbrenner et al. [12]. Therefore, the operational conditions in this period were selected on the basis of obtaining good solubility at low pressures.

According to the solubility values in the literature, the estimated solubility of $CoCp_2$ in CO_2 at 70 ºC and 11.0 MPa is 0.336 g/L [12].
Experiments were performed with two different initial amounts of precursor: 48 and 7 mg and the final loading of cobalt in the samples for both situations were Co > 4% wt. and Co < 1% wt. respectively, determined by ICP-OES.
These two initial amounts of precursor corresponded to a maximum ''theoretical'' concentration in the supercritical phase of 0.48 and 0.07 g/L, respectively. Therefore, in the first kind of experiments, the supercritical phase was saturated, and 14.4 mg of $CoCp_2$ remained in a solid state after the first 3 h, whereas in the other case, concentration was far below the solubility value, and the precursor located in the reactor was solubilized in the supercritical phase. After this period, thermal decomposition took place at 200 ºC and 16.0 MPa in the supercritical CO_2 phase during 3 h.
Nitrogen adsorption and desorption experiments together with SAXS measurements were employed to study the effect of $scCO_2$ and the addition of cobalt on the surface area, mesoporous hexagonal arrangement and pore distribution of the prepared samples.
Table 1 presents the results obtained by N_2 adsorption/desorption measurements for the mesoporous supports, and the Co(X)/MCM-41 and Co(X)/Al-MCM-41 samples. The SAXS and ICP-OES results are also shown. All the solids gave typical type-IV isotherms with a sharp inflection at relative pressure $P/P_0 > 0.3$, characteristic of capillary condensation, which indicates the uniformity of the mesoporous size distributions.

Table 1. Textural properties of the prepared samples.

Samples	Co (wt%)[(a)]	a_{BET} (m^2/g)	Pore size (nm)	d_{100}[(b)]	a_0[(c)]
MCM-41 calcined	0	1295	4.6	3.7	4.3
Co(0.6)/MCM41	0.63	1183	4.5	3.7	4.3
Co(4.3)/MCM41	4.34	1034	3.9	3.7	4.3
Al-MCM-41 calcined	0	807	4.8	3.7	4.3
Co(0.8)/Al-MCM-41	0.82	752	4.1	3.4	3.9
Co(5)/Al-MCM-41	5.10	709	3.9	3.4	3.9

[a] Determined by ICP-OES.
[b] Interplanar distance, nm *($d_{100} = \lambda/2 \cdot \sin\theta$)*
[c] Unit cell parameter, nm *($a_0 = 1.1547 \cdot d_{100}$)*

It is noticeable that the addition of aluminium to the MCM-41 support produced a drop of approximately 38% in the a_{BET} while the pore size remained constant. In addition, from the same amount of precursor, the content of Co deposited on Al-MCM-41 was slightly higher compared to the support without aluminium, (0.8 against 0.6% and 5.0 against 4.3 %). It is known that the addition of Al to pure silica is performed to give more acidity to the neutral character of the MCM-41 structure. Therefore, a mild interaction between aluminium and cobalt is likely to occur. The deposition of Co supposed a reduction in the a_{BET}, but this diminution is lower for Al-MCM-41 than for MCM-41, as it is shown in table 1. The average pore size has been obtained from the BJH analysis (values in table 1), and pore size slightly decreased with the increase of the cobalt loading. This fact could be attributed to the addition of cobalt nanoparticles inside of the mesopores.
The results obtained by SAXS for the Co(x)/MCM-41 and Co(x)/Al-MCM-41 samples are shown in Fig. 2A and B, respectively.

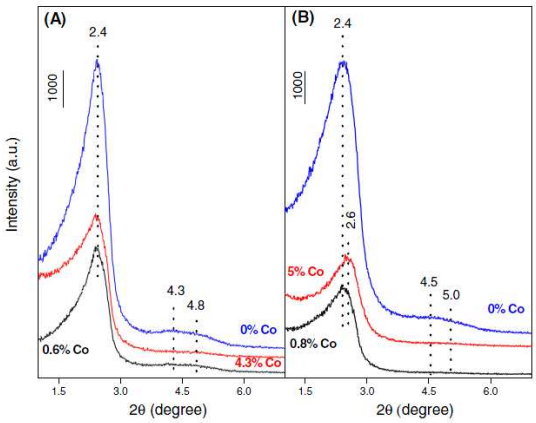

Figure 2. SAXS results for: (A) Co(X)/MCM-41 and (B) Co(X)/Al-MCM-41

The appearance of a strong diffraction peak at 2.4º is characteristic of the (1 0 0) plane of the supports and indicates an ordered pore structure for MCM-41 and Al-MCM-41. The major intensity of this peak for the support without aluminium should be noticed. The weak diffraction peaks close to 4.3º and 5.0º which correspond to the (1 1 0) and (2 0 0) planes verify the synthesized mesoporous structure. This confirms that the synthesized spherical samples have a hexagonal arrangement. The interplanar distance in the (1 0 0) direction, 'd100', was calculated by Bragg's Law ($\lambda = 2 \cdot d_{hkl} \cdot sin\theta$) and the unit cell parameter 'a0' was also obtained, indicating the distance between the center of two adjacent pores in the hexagonal structure ($a_0 = 2 \cdot d_{100} / \sqrt{3}$) [11]. Both parameters are included in Table 1. As shown in Fig. 2A, the pore structure of both supports remains unchanged after introducing the Co atoms.

Characterization of the deposited cobalt nanoparticles

The SEM images in Fig. 3 show that the morphologies of synthesized MCM-41 (Fig. 3A) and Al-MCM-41 meso-materials are spherical, and the mean size is around 500 nm. The temperature and surfactant concentration used during the synthesis process are factors which affect the shape of the prepared samples.

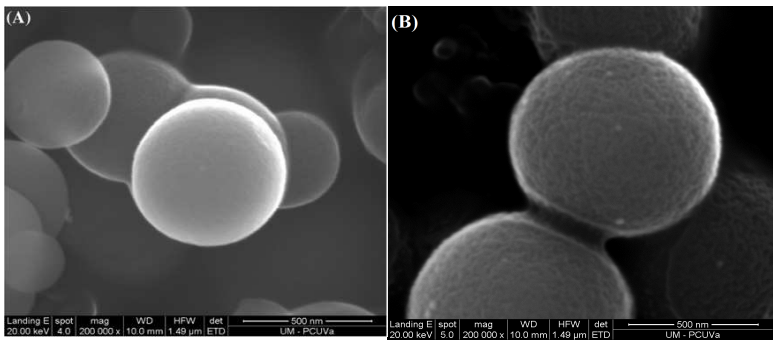

Figure 3. SEM images of calcined supports (A) MCM-41 and (B) Co(X)/MCM-41

After the Co addition by supercritical CO_2, the spherical morphology of the mesoporous particles is remained (Fig. 3B). Individual nanoparticles cannot be directly observed using the secondary electron mode of the SEM. However, when the imaging is performed using the backscattered electron (BSE) mode, the presence of high electron dense areas, i.e. metallic particles, can be inferred. Fig. 4A and B shows the BSE images obtained from the Co(5)/Al-

MCM-41 and Co(4.3)/MCM-41 samples, respectively. In the BSE image bright patches are observed, which indicate high electron dense areas, where increased brightness is due to the presence of a metal. The areas of high electron density appear well dispersed and correspond to cobalt nanoparticles with approximately 20 nm of diameter.

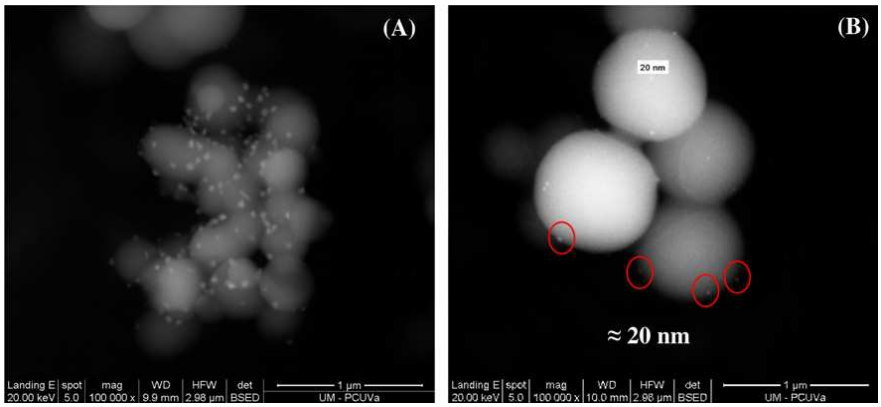

Figure 4. BSE SEM images of (A) Co(5)/Al-MCM-41 and (B) Co(4.3)/MCM-41

Figs. 5 and 6 show the X-ray mapping results in SEM images obtained for Co(0.6)/MCM-41 and Co(4.3)/MCM-41, respectively. Different colors in grayscale are associated with diverse emission lines. In this way, each color in the picture refers to the single emission energy of the interesting element. When the Co loading is 0.6 wt.%, a homogeneous distribution of different cobalt species in mesoporous spheres is observed. However, when the cobalt content increases to 4.3 wt.%, spherical nanoparticles on the outer surface of MCM-41 support are observed. The diameter of these nanoparticles varies between 10 and 15 nm.

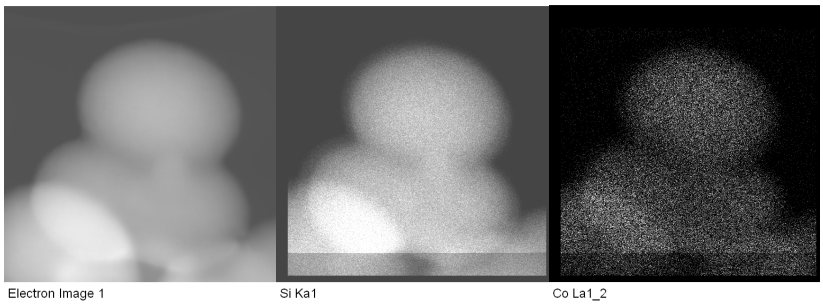

Figure 5. X-ray TEM/EDX mapping for Co(0.6)/MCM-41: (A) electron image, (B) Co κα and (C) Si κα

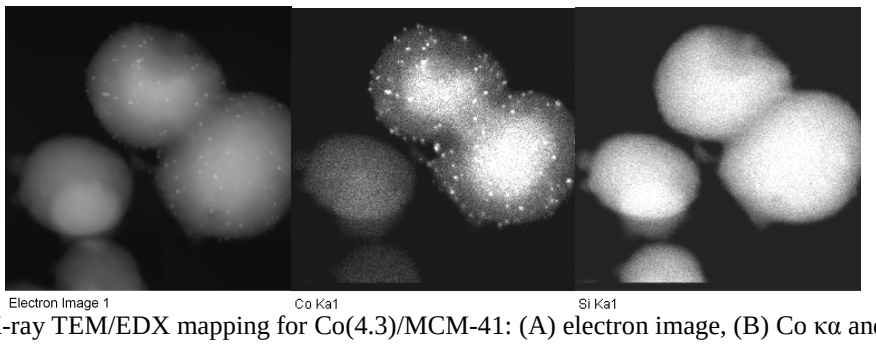

Figure 6. X-ray TEM/EDX mapping for Co(4.3)/MCM-41: (A) electron image, (B) Co κα and (C) Si κα

As previously mentioned, for a Co content of 4.3 wt.%, the initial amount of $CoCp_2$ located in the reactor is higher than the solubility value, and the solid precursor remains without

dissolution after the dissolution and impregnation stage. Therefore, during the decomposition stage, the deposition of cobalt nanoparticles also takes place on the outer surface.
From these results, it can be observed that with a low Co loading on both supports, the nanoparticles locate inside the mesoporous spheres. When the cobalt load increases and the initial concentration is higher than the solubility value in the supercritical phase, the nanoparticles can be observed both inside the spheres and also on the surface of the MCM-41 and Al-MCM-41 supports.

In order to corroborate the outer nanoparticle sizes obtained from SEM and to differentiate the cobalt species, TEM analysis was employed. Fig. 7 shows the TEM images of cobalt deposited on the mesoporous supports. TEM micrographs (Fig. 7) also show the presence of Co nanoparticles on the surface, with diameters between 15 and 20 nm.

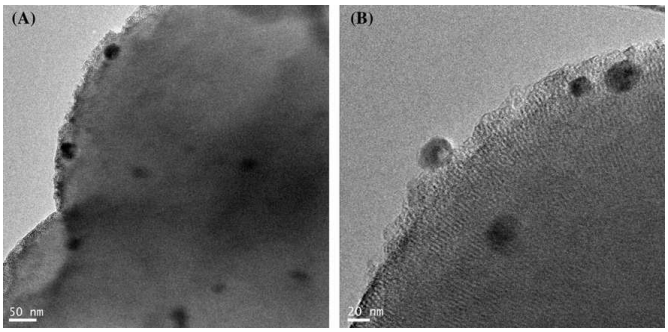

Figure 7. TEM images of (A) Co(4.3)/MCM-41 and (B) Co(5)/Al-MCM-41

The presence of Co_3O_4 nanoparticles on Co(X)/Al-MCM41 could be determined by Raman spectroscopy. Fig. 8 presents the Raman spectra of the Co(X)/MCM-41 and Co(X)/Al-MCM-41 samples. The spectra of the samples with lower cobalt loading, Co(0.6)/MCM- 41 and Co(0.8)/Al-MCM-41, present several bands at 495, 602, 818 and 973 cm^{-1} corresponding to the mesoporous supports. In addition, a small signal appears at 690 cm^{-1}. At higher cobalt loading (spectra (b) and (d)), the intensity at 690 cm^{-1} increases and a new signal appears at 520 cm^{-1}. Both signals correspond to the main bands of the Co_3O_4 spinel phase [14].

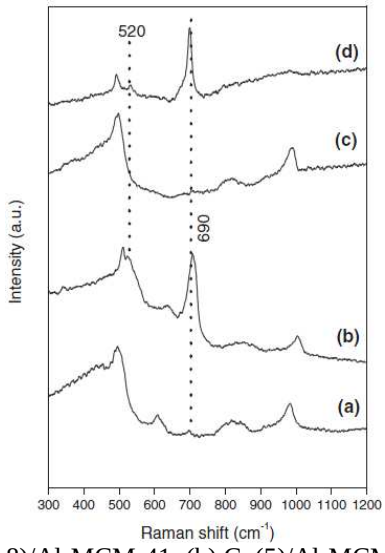

Figure 8. Raman spectra (a) Co(0.8)/Al-MCM-41; (b) Co(5)/Al-MCM-41; (c) Co(0.6)/MCM-41 and (d) Co(4.3)/MCM-41

CONCLUSIONS

Supercritical CO_2 is a suitable, simple and effective medium to incorporate cobalt nanoparticles into mesoporous MCM-41 and Al-MCM-41 materials. Cobalt oxide nanoparticles were uniformly dispersed in both supports. The experimental results show that it is important to control the initial precursor concentration during the first synthesis stage. This value should be lower than the solubility limit in order to prevent particle growth on the outer surface. Moreover, the presence of aluminium in the Al-MCM-41 support allowed the incorporation of a higher amount of cobalt compared to the Al-free support. TEM, LSR and XPS indicated the presence of well-dispersed CoO and Co_3O_4 nanoparticles inside both substrates, with an average size of less than 4 nm. When the cobalt content was close to 5%, "extra" nanoparticles 10-20 nm in size appeared on their outer surface. This is because the initial amount of the precursor war higher than the solubility value with $scCO_2$. No significant changes were observed in the hexagonal arrangement and specific surface area of mesoporous supports after adding a high content of cobalt nanoparticles (close to 5%)

REFERENCES

[1] LINSSEN T., CASSIERS K., COOL P., VANSANT E.F., Adv. Colloid Interface Sci. Vol. 103, **2003**, p.121
[2] LEE S., PARK B., BYEON F., CHANG H., Chem. Mater., Vol. 18, No. 24, **2006**, p.5631
[3] RICE R.L., AMOLD D.C., SHAW T., IACOPINA D., QUINN A.J., AMENITSCH H., HOLMES J.D., MORRIS M.A., Adv. Funct. Mater. Vol. 17, **2007**, p.133
[4] WU Q., HU X., YUE P.L., ZHAOB X.S., LUB G.Q., Appl. Catal. B: Environ. Vol. 32, **2001**, p.151.
[5] CHALIHA S., BHATTACHARYYA G., Catalysis Today Vol. 141, **2009**, p.225
[6] SZEGEDI A., POPOVA M., DIMITROVA A., CHERKEZKOVA-ZHELEVA Z., MITOV I., Micropor. Mesopor. Mater. Vol. 136, **2010**, p.106–114
[7] SZEGEDI A., POPOVA M., MINCHEV C., J. Mater. Sci. Vol. 44. **2009**, p.6710–6716
[8] GHAMPSON I.T., NEWMAN C., KONG L., PIER E., HURLEY K.D. POLLOCK R.A., WALSH B.R., GOUNDIE B., WRIGHT J., WHEELER M.C., MEULENBERG R.W., DESISTO W.J., FREDERICK B.J., AUSTIN R.N., Appl. Catal. A: Gen. Vol. 388, **2010**, p.57–67
[9] GONZALEZ O., PEREZ H., NAVARRO P., ALMEIDA L.C., PACHECO J.G., MONTES M., Catal. Today Vol. 148, **2009**, p.140–147
[10] ASPROMONTE S. G., SASTRE A., BOIX A.V., COCERO M.J., ALONSO E., Microporous and Mesoporous Materials, doi:10.1016/j.micromeso.**2011**.07.014
[11] SZEGEDI A., KONYA Z., MEHN D., SOLYMAR E., PAL-BORBELY G., HORVATH Z.E., BIRO L.P., KIRICSI I., Applied Catalysis A: General Vol. 272, **2004**, p.257–266
[12] ASCHENBRENNER O., KEMPER S., DAHMEN N., SCHABER K., DINJUS E., J. Supercrit. Fluids Vol. 41, **2007**, p.179–186
[13] HUNDE E.T., WATKINS J.J., Chem. Mater. Vol. 16, **2004**, p.498–503
[14] BOIX A.V., ASPROMONTE S.G., MIRO E.E., Appl. Catal. A: Gen. Vol. 341, **2008**, p.26–34